Available online at www.sciencedirect.com

ScienceDirect

IFAC PapersOnline CONFERENCE PAPER ARCHIVE

IFAC PapersOnLine 58-6 (2024) 101–106

Generalized Maxwell viscoelasticity for geometrically exact strings: Nonlinear port-Hamiltonian formulation and structure-preserving discretization

P. L. Kinon * **T. Thoma** ** **P. Betsch** * **P. Kotyczka** **

* *Institute of Mechanics, Karlsruhe Institute of Technology (KIT), Otto-Ammann-Platz 9, 76131 Karlsruhe, Germany (email: {philipp.kinon, peter.betsch}@kit.edu)*

** *TUM School of Engineering and Design, Technical University of Munich (TUM), Boltzmannstr. 15, 85748 Garching, Germany (email: {tobias.thoma, kotyczka}@tum.de)*

Abstract: This contribution proposes a nonlinear and dissipative infinite-dimensional port-Hamiltonian (PH) model for the dynamics of geometrically exact strings. The mechanical model provides a description of large deformations including finite elastic and inelastic strains in a generalized Maxwell model. It is shown that the overall system results from a power-preserving interconnection of PH subsystems. By using a structure-preserving mixed finite element approach, a finite-dimensional PH model is derived. Eventually, midpoint discrete derivatives are employed to deduce an energy-consistent time-stepping method, which inherits discrete-time dissipativity for the irreversible system. An example simulation illustrates the numerical properties of the present approach.

Keywords: Nonlinear port-Hamiltonian systems, generalized Maxwell model, structure-preserving discretization, mixed finite elements, discrete gradients.

1. INTRODUCTION

The class of port-Hamiltonian (PH) systems has become increasingly important across multiple research fields dealing with modeling and control of complex dynamical systems, see e.g. Duindam et al. (2009). A major benefit of the PH representation is the explicit formulation of power interfaces, so-called ports, which allows for an intrinsically energy-consistent interconnection, thus facilitating the modular composition of subsystems. Since many technical systems are modeled by partial differential equations, the theory of infinite-dimensional PH systems has been extended in recent years, see Rashad et al. (2020) for a review. Among various physical disciplines, PH formulations have also been proposed for mechanics.

The structural elements of strings are particularly interesting and are widely used in control and modeling of multibody systems (cf. Ströhle and Betsch (2022); Kinon et al. (2023a)). Strings can be found in a large variety of systems such as cranes, cable robots or satellite systems. Accordingly, they are interconnected with their environment, which can be described beneficially in the PH framework. So far, works on geometrically exact strings have been restricted to purely elastic materials: linear elasticity in Thoma and Kotyczka (2022) and nonlinear elasticity in Kinon et al. (2023a). However, modeling inelastic processes plays a crucial role for the realistic simulation of mechanical systems, see Simo and Hughes (2006). Many works from structural and multibody dynamics deal with the Kelvin-Voigt model (e.g. Linn et al. (2013)), which is not able to reproduce the relaxation test. Recently, more advanced models (such as the generalized Maxwell model) are investigated, see e.g. Bauchau and Nemani (2021).

In this contribution we make use of an infinite-dimensional, nonlinear and dissipative PH model related to Mehrmann and Morandin (2019); Mehrmann and Zwart (2024). We thus extend the existing description of geometrically exact strings to viscoelasticity, introduce the (distributed) generalized Maxwell model to the PH context and explore the model's advantages concerning PH interconnection. With respect to the numerical discretization, the mixed finite element method has been employed to establish an approximate model under preservation of the PH structure, see Cardoso-Ribeiro et al. (2021), retaining the ports with their causality on the discrete level. Lastly, we propose an energy-consistent time discretization extending the one in Kinon et al. (2023b). It is based on the midpoint discrete gradient due to Gonzalez (1996) and can be related to the *discrete-gradient pairs* by Schulze (2023). The resulting scheme inherits the dissipativity property of the underlying continuous model.

2. INFINITE-DIMENSIONAL MODEL

In this section, we derive a model for geometrically exact strings, with a new extension to viscoelastic material using

⋆ The financial support by the DFG (German Research Foundation) – project number 388118188 – is gratefully acknowledged.

10.1016/j.ifacol.2024.08.264

a generalized Maxwell model. After briefly recalling the purely hyperelastic model from Kinon et al. (2023a), we present a PH formulation of the parallel connection of distributed visco-elastic branches according to the generalized Maxwell model. Eventually, a power-preserving interconnection of both systems yields the final model.

2.1 Purely hyperelastic model

We consider a one-dimensional undeformed (material) string configuration $\Omega \subset \mathbb{R}^d$ of length $L \in \mathbb{R}_{>0}$ and its current (spatial) configuration $\Omega_t \subset \mathbb{R}^d$, where $d \in \{1,2,3\}$ is the spatial dimension. Correspondingly, the position vector $\boldsymbol{r} : \mathbb{S} \times \mathbb{T} \to \Omega_t$ is introduced, depending on the material arc-length coordinate $s \in \mathbb{S} = [0, L]$ and on time $t \in \mathbb{T} \subset \mathbb{R}_{\geq 0}$, see Fig. 1 for an illustration. The balance of linear momentum

$$\rho A \ddot{\boldsymbol{r}}(s,t) = \partial_s \boldsymbol{n}(s,t) + \boldsymbol{b} + \boldsymbol{f}(s,t) \tag{1}$$

includes the constant mass density $\rho \in \mathbb{R}_{\geq 0}$, cross-section area $A \in \mathbb{R}_{\geq 0}$, constant body forces per unit length $\boldsymbol{b} \in \mathbb{R}^d$, and distributed input forces per unit length $\boldsymbol{f} \in \mathbb{R}^d$. The temporal partial derivative of a any function $\square$ is denoted $\dot{\square} := \partial_t \square$. Moreover, the contact force $\boldsymbol{n}(s,t) : \mathbb{S} \times \mathbb{T} \to \mathbb{R}^d$ has tangential direction, i.e.,

$$\boldsymbol{n}(s,t) = S(s,t) \partial_s \boldsymbol{r}(s,t), \tag{2}$$

where the stress-type quantity $S : \mathbb{S} \times \mathbb{T} \to \mathbb{R}$ has been introduced.[1] In similarity to (2), we assume that the distributed input forces are restricted to purely tangential contributions

$$\boldsymbol{f} = 2\partial_s(\frac{1}{2} S_u \partial_s \boldsymbol{r}) \tag{3}$$

with $S_u(s,t)$ the stress-type input. For the kinematic description we consider the scalar strain measure

$$C = \partial_s \boldsymbol{r} \cdot \partial_s \boldsymbol{r}, \tag{4}$$

where $C = 1$ corresponds to a state without elongation. For the nonlinear elastic constitutive modeling with finite strains, a non-quadratic strain energy density function

$$W(C) = \frac{EA}{4}(C - \ln(C) - 1), \tag{5}$$

with $E \in \mathbb{R}_{>0}$ the constant axial stiffness parameter, is considered and is bounded from below by $W(1) = 0$. See Kinon et al. (2023a) for a model with linear stress-strain relation due to St.-Venant-Kirchhoff. The axial stress is derived via differentiation as

$$S := 2\frac{\mathrm{d}W}{\mathrm{d}C} = 2W'(C). \tag{6}$$

The total energy of a geometrically exact string is described in terms of the state vector

$$\boldsymbol{x}_1 = (\boldsymbol{r}, \boldsymbol{v}, C) \in \mathbb{R}^{2d+1} \tag{7}$$

by its Hamiltonian

$$H_1[\boldsymbol{x}_1] = \int_0^L \left(\frac{\rho A}{2} \boldsymbol{v} \cdot \boldsymbol{v} + W(C) - \boldsymbol{r} \cdot \boldsymbol{b} \right) \mathrm{d}s, \tag{8}$$

which is the sum of kinetic energy and potential energy. Correspondingly, the variational derivatives yield

$$\delta_{\boldsymbol{x}_1} H_1[\boldsymbol{x}_1] = (-\boldsymbol{b}, \rho A \boldsymbol{v}, W'(C)) \in \mathbb{R}^{2d+1}. \tag{9}$$

Taking the balance of linear momentum (1), the kinematic relation $\dot{\boldsymbol{r}} = \boldsymbol{v}$, and the strain rate derived from

[1] We now drop both spatial and temporal arguments for the sake of brevity and only use them where the explicit mention is helpful.

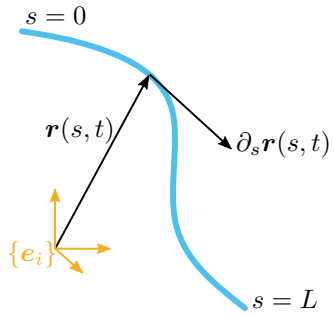

Fig. 1. Spatial string configuration.

(4), the state differential equations represent an infinite-dimensional version of the formulation by Mehrmann and Morandin (2019)

$$\begin{aligned} \mathcal{E}_1 \dot{\boldsymbol{x}}_1 &= \mathcal{J}_1(\boldsymbol{x}_1)\boldsymbol{z}_1 + \mathcal{B}(\boldsymbol{x}_1)u_1 \ , \quad \text{where} \quad \mathcal{E}_1^{\mathsf{T}} \boldsymbol{z}_1 = \delta_{\boldsymbol{x}_1} H_1 \ , \\ y_1 &= \mathcal{B}^*(\boldsymbol{x}_1)\boldsymbol{z}_1 \ , \end{aligned} \tag{10}$$

see also Mehrmann and Zwart (2024) for a recent linear operator-theoretic approach. Note that (10) is specified by $\mathcal{E}_1 = \mathrm{diag}\{\boldsymbol{I}, \rho A \boldsymbol{I}, 1\}$, $\boldsymbol{z}_1 = (-\boldsymbol{b}, \boldsymbol{v}, \frac{1}{2}S)$, the formally skew-adjoint ($\mathcal{J}_1 = -\mathcal{J}_1^*$) matrix differential operator

$$\mathcal{J}_1(\boldsymbol{x}_1) = \begin{bmatrix} \boldsymbol{0} & \boldsymbol{I} & 0 \\ -\boldsymbol{I} & \boldsymbol{0} & 2\partial_s(\square\, \partial_s \boldsymbol{r}) \\ \boldsymbol{0}^{\mathsf{T}} & 2\partial_s \boldsymbol{r} \cdot \partial_s \square & 0 \end{bmatrix}, \tag{11}$$

which has a similar state-dependent structure as the one in Brugnoli et al. (2021) for von Kármán beams, and

$$\mathcal{B}(\boldsymbol{x}_1) = \begin{bmatrix} \boldsymbol{0} \\ 2\partial_s(\square\, \partial_s \boldsymbol{r}) \\ 0 \end{bmatrix}, \quad \mathcal{B}^*(\boldsymbol{x}_1) = \begin{bmatrix} \boldsymbol{0}^{\mathsf{T}} & -2\partial_s \boldsymbol{r} \cdot \partial_s \square & 0 \end{bmatrix}. \tag{12}$$

See Kinon et al. (2023a) for details without the distributed port, and the Appendices for two related formulations. In App. A the description of inextensible strings yielding partial DAEs is covered and App. B proposes a representation in an extended state space, with a "standard" canonical differential operator, known from systems of two conservation laws.

Lastly, the power balance is shown as

$$\begin{aligned} \dot{H}_1 &= \int_0^L \delta_{\boldsymbol{x}_1} H_1 \cdot \dot{\boldsymbol{x}}_1 \, \mathrm{d}s = \int_0^L \boldsymbol{z}_1 \cdot \mathcal{E}_1 \dot{\boldsymbol{x}}_1 \, \mathrm{d}s \\ &= \int_0^L \boldsymbol{z}_1 \cdot \mathcal{J}_1 \boldsymbol{z}_1 \, \mathrm{d}s + \int_0^L \boldsymbol{z}_1 \cdot \mathcal{B} u_1 \, \mathrm{d}s, \\ &= \boldsymbol{u}_\partial \cdot \boldsymbol{y}_\partial + \int_0^L u_1 \cdot y_1 \, \mathrm{d}s \end{aligned} \tag{13}$$

in order to complete the PH system representation.[2] Therein, the boundary port $(\boldsymbol{u}_\partial, \boldsymbol{y}_\partial)$ has been defined due to pure Neumann boundary conditions (BCs) with

$$\boldsymbol{u}_\partial(t) = \begin{bmatrix} -\boldsymbol{n}_{\mathrm{tot}}(0,t) \\ \boldsymbol{n}_{\mathrm{tot}}(L,t) \end{bmatrix}, \quad \boldsymbol{y}_\partial(t) = \begin{bmatrix} \boldsymbol{v}(0,t) \\ \boldsymbol{v}(L,t) \end{bmatrix}, \tag{14}$$

where $\boldsymbol{n}_{\mathrm{tot}} = S_{\mathrm{tot}} \partial_s \boldsymbol{r}$, with $S_{\mathrm{tot}} := S + S_u$, is the total contact force. The collocated distributed input-output pair in (13) is $(u_1, y_1) = (\frac{1}{2}S_u, -\dot{C})$, which have the dimension of a stress and strain-rate, respectively.

[2] Here, integration by parts along with (10) and (12) have been used.

2.2 Distributed generalized Maxwell viscoelasticity

We now introduce viscoelastic material behavior. Particularly, we assume an *internal variable model*: the generalized Maxwell model with the rheological model from Fig. 2, which consists of an elastic element and m viscous Maxwell elements in parallel. It is also referred to as *generalized relaxation model*, see (Simo and Hughes, 2006, Ch. 10). In this context, each additional branch introduces new material parameters, allowing for a more precise modeling of the time-dependent material behavior. Due to the model's structure, the total strain in each branch is equal to the overall total strain C_{tot}. Correspondingly, C_{tot} is also the strain in the purely elastic branch, which corresponds to the undamped string model with strain C from (4).

In each viscous branch, the elastic strain C_i^{el} and the inelastic strain α_i must add to the total strain $C_{\text{tot}}(s)$,

$$C_i^{\text{el}}(s) + \alpha_i(s) = C_{\text{tot}}(s), \quad i = 1, \dots, m, \tag{15}$$

or, in terms of the strain rates,

$$\dot{C}_i^{\text{el}}(s) + \dot{\alpha}_i(s) = \dot{C}_{\text{tot}}(s), \quad i = 1, \dots, m. \tag{16}$$

The parallel interconnection implies the addition of the stresses of each viscoelastic branch as

$$S_{\text{v}}(s) = \sum_{i=1}^{m} S_i(s), \tag{17}$$

which adds with the stress in the purely elastic branch to $S_{\text{tot}}(s) = S_{\text{v}}(s) + S(s)$. Moreover, at each (distributed) dashpot element, inelastic strains and stresses are related by the constitutive relation

$$\dot{\alpha}_i(s) = \frac{1}{\eta_i A} S_i(s), \tag{18}$$

where $\eta_i \in \mathbb{R}_{>0}$ is the dynamic viscosity assigned to this branch. The stresses (which are equal in a branch), are obtained similar to (6) from a constitutive relation defined by $S_i := 2\tilde{W}_i'(C_i^{\text{el}})$. Choosing a suitable hyperelastic energy density $\tilde{W}_i(C_i^{\text{el}})$ as in (5), a stiffness parameter E_i is assigned to every elastic element. [3] The dissipation functional (see Simo and Hughes (2006)) for the generalized Maxwell model is defined here as

$$\mathcal{D} := \int_0^L \sum_{i=1}^{m} \frac{1}{2\eta_i A} S_i^2(s) \, \mathrm{d}s. \tag{19}$$

With the total energy

$$H_2[\boldsymbol{x}_2] = \int_0^L \sum_{i=1}^{m} \tilde{W}_i(C_i^{\text{el}}) \, \mathrm{d}s, \quad \boldsymbol{x}_2 = (C_1^{\text{el}}, \dots, C_m^{\text{el}}) \in \mathbb{R}^m, \tag{20}$$

and the variational derivatives

$$\delta_{\boldsymbol{x}_2} H_2 = (\tilde{W}_1'(C_1^{\text{el}}), \dots, \tilde{W}_m'(C_m^{\text{el}})) \tag{21}$$

the above equations can be combined to obtain the dynamics of the m viscoelastic Maxwell branches in purely dissipative PH form [4]

$$\begin{aligned} &\dot{\boldsymbol{x}}_2 = -\mathcal{R}_2 \boldsymbol{z}_2 + \mathbf{1}\dot{C}_{\text{tot}}, \quad \text{where } \boldsymbol{z}_2 = \delta_{\boldsymbol{x}_2} H_2 \\ &\frac{1}{2} S_{\text{v}} = \mathbf{1}^{\mathsf{T}} \boldsymbol{z}_2, \end{aligned} \tag{22}$$

[3] To obtain consistency with a purely elastic string model with axial stiffness $\overline{EA}$, it is required that $EA + \sum_i^m E_i A = \overline{EA}$.

[4] A more standard approach in computational viscoelasticity defines the state via the inelastic strains α_i and would yield a slightly different PH model.

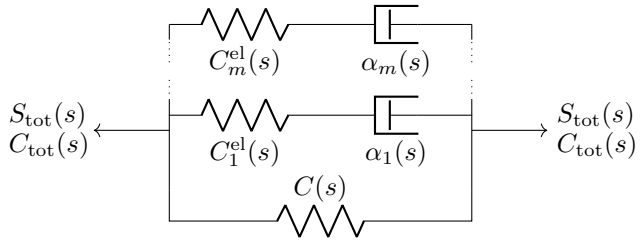

Fig. 2. Generalized Maxwell model.

with $\boldsymbol{z}_2 = (\frac{1}{2}S_1, \dots, \frac{1}{2}S_m)$, $\mathcal{R}_2 = \operatorname{diag}\{\frac{2}{\eta_1 A}, \dots, \frac{2}{\eta_m A}\}$, $\mathbf{1}^{\mathsf{T}} = [1, \dots, 1]$ and the distributed input-output pair $(u_2, y_2) = (\dot{C}_{\text{tot}}, \frac{1}{2}S_{\text{v}})$. Eventually, the dissipation inequality

$$\dot{H}_2 = -\mathcal{D} + \int_0^L u_2 \cdot y_2 \, \mathrm{d}s \le \int_0^L u_2 \cdot y_2 \, \mathrm{d}s \tag{23}$$

is induced, using (19) as well as $\mathcal{D}[\boldsymbol{z}_2] = \int_0^L \boldsymbol{z}_2 \cdot \mathcal{R}_2 \boldsymbol{z}_2 \, \mathrm{d}s$. [5]

2.3 Interconnection and viscoelastic string model

According to the aforementioned model (see Fig. 2), we interconnect the purely elastic model and the m viscoelastic Maxwell branches via the conditions $S_u = S_{\text{v}}$, $\dot{C} = \dot{C}_{\text{tot}}$, i.e., the total stress of the visco-elastic elements acts as distributed stress input to the purely elastic string, while kinematic continuity of the strains is given. In terms of the above-defined (u_1, y_1) and (u_2, y_2), this reads

$$\begin{bmatrix} u_1 \\ u_2 \end{bmatrix} = \begin{bmatrix} 0 & 1 \\ -1 & 0 \end{bmatrix} \begin{bmatrix} y_1 \\ y_2 \end{bmatrix}, \tag{24}$$

i.e., a standard power-preserving (gyrator) interconnection of two passive systems.

Theorem 1. By combining the PH models (10), (22) with (24), the boundary controlled PH model of the geometrically exact string with generalized Maxwell visco-elasticity and imposed Neumann BCs is given by

$$\mathcal{E}\dot{\boldsymbol{x}} = (\mathcal{J}(\boldsymbol{x}) - \mathcal{R})\boldsymbol{z}\,, \qquad \mathcal{E}^{\mathsf{T}}\boldsymbol{z} = \delta_{\boldsymbol{x}} H\,, \tag{25}$$

with $\mathcal{E} = \operatorname{diag}\{\mathcal{E}_1, \boldsymbol{I}\}$, states $\boldsymbol{x}_1 = (\boldsymbol{x}_1, \boldsymbol{x}_2) \in \mathbb{R}^{2d+1+m}$, vector $\boldsymbol{z} = (\boldsymbol{z}_1, \boldsymbol{z}_2)$ and boundary port $(\boldsymbol{u}_\partial, \boldsymbol{y}_\partial)$ according to (14), as well as consistent initial conditions. The formally skew-adjoint system operator and the dissipation matrix are

$$\mathcal{J}(\boldsymbol{x}) = \begin{bmatrix} \mathbf{0} & \boldsymbol{I} & 0 & 0 \\ -\boldsymbol{I} & \mathbf{0} & 2\partial_s(\square\, \partial_s \boldsymbol{r}) \cdots & 2\partial_s(\square\, \partial_s \boldsymbol{r}) \\ \mathbf{0} & 2\partial_s \boldsymbol{r} \cdot \partial_s \square & 0 & 0 \\ & \vdots & & \\ \mathbf{0} & 2\partial_s \boldsymbol{r} \cdot \partial_s \square & 0 & 0 \end{bmatrix}. \tag{26}$$

and $\mathcal{R} = \operatorname{diag}\{\mathbf{0}, \mathcal{R}_2\}$. The Hamiltonian is the sum of (8) and (20),

$$H[\boldsymbol{x}] = H_1[\boldsymbol{x}_1] + H_2[\boldsymbol{x}_2], \tag{27}$$

and satisfies the power balance

$$\dot{H} = \boldsymbol{u}_\partial \cdot \boldsymbol{y}_\partial - \mathcal{D}[\boldsymbol{z}] \le \boldsymbol{u}_\partial \cdot \boldsymbol{y}_\partial, \tag{28}$$

[5] With initial conditions $\boldsymbol{x}_2(0)$ and the distributed input $\dot{C}_{\text{tot}}(s)$ acting on the complete domain $\mathbb{S}$, no additional BCs need to be specified. This is in accordance with (23), which comes without boundary terms. This is clear from the $\mathcal{R}_2$ being constant.

with the non-negative dissipation functional, being identical with (19) taking part in (23), such that

$$\mathcal{D}[\boldsymbol{z}] = \int_0^L \boldsymbol{z} \cdot \mathcal{R}\boldsymbol{z} \, \mathrm{d}s \geq 0. \tag{29}$$

Proof. The form of the operators follows from direct substitution. The PH structure, with formal skew-adjointness of $\mathcal{J}$, is a direct consequence of the power-conserving interconnection, just as the power balance, which follows from adding (13) and (23).

3. STRUCTURE-PRESERVING DISCRETIZATION

3.1 Spatial discretization

A mixed finite element approach yields a semi-discrete state space model that fits again into the PH framework. To this end, the weak form pertaining to (25) is deduced using standard procedures as [6]

$$(\delta\boldsymbol{b}, \dot{\boldsymbol{r}} - \boldsymbol{v})_\Omega = 0, \tag{30a}$$

$$(\delta\boldsymbol{v}, \rho A\dot{\boldsymbol{v}} - \boldsymbol{b})_\Omega + (\partial_s(\delta\boldsymbol{v}), S_{\mathrm{tot}}\partial_s\boldsymbol{r})_\Omega - [\boldsymbol{n}_{\mathrm{tot}} \cdot \delta\boldsymbol{v}]_0^L = 0, \tag{30b}$$

$$\Big(\delta S, \dot{C} - 2\partial_s\boldsymbol{r} \cdot \partial_s\boldsymbol{v}\Big)_\Omega = 0, \tag{30c}$$

$$\left(\delta S_i, \dot{C}_i^{\mathrm{el}} - 2\partial_s\boldsymbol{r} \cdot \partial_s\boldsymbol{v} + \frac{1}{\eta_i A} S_i\right)_\Omega = 0, \tag{30d}$$

for arbitrary test functions $\delta\boldsymbol{b}, \delta\boldsymbol{v}, \delta S$ and δS_i from appropriate spaces and $i = 1, \ldots, m$. Note that constitutive weak forms corresponding to $\mathcal{E}^\mathsf{T}\boldsymbol{z} = \delta_{\boldsymbol{x}} H$ given by

$$(\delta C, S - 2W'(C))_\Omega = 0, \tag{30e}$$

$$\Big(\delta C_i^{\mathrm{el}}, S_i - 2\tilde{W}_i'(C_i^{\mathrm{el}})\Big)_\Omega = 0, \tag{30f}$$

for $i = 1, \ldots, m$ with appropriate δC, δC_i^{el}, are appended to close the set of equations.

Now, the string domain is divided into n_{el} finite elements and we approximate $\boldsymbol{r}$,$\boldsymbol{v}$,$\boldsymbol{b}$ via C^0-continuous, linear Lagrangian shape functions and C, S, C_i^{el}, S_i via elementwise constant, discontinuous ansatz functions. Considering a Bubnov Galerkin approach, the corresponding test functions are restricted to the same ansatz spaces. This yields

$$\dot{\hat{\boldsymbol{r}}} = \hat{\boldsymbol{v}}, \tag{31a}$$

$$\boldsymbol{M}_\rho\dot{\hat{\boldsymbol{v}}} = \boldsymbol{M}\hat{\boldsymbol{b}} - \boldsymbol{K}(\hat{\boldsymbol{r}})\hat{\boldsymbol{S}} - \sum_{i=1}^m \boldsymbol{K}(\hat{\boldsymbol{r}})\hat{\boldsymbol{S}}_i + \boldsymbol{B}_\partial\hat{\boldsymbol{u}}_\partial, \tag{31b}$$

$$\boldsymbol{M}_S\dot{\hat{\boldsymbol{C}}} = 2\boldsymbol{K}(\hat{\boldsymbol{r}})^\mathsf{T}\hat{\boldsymbol{v}}, \tag{31c}$$

$$\boldsymbol{M}_S\dot{\hat{\boldsymbol{C}}}_i^{\mathrm{el}} = 2\boldsymbol{K}(\hat{\boldsymbol{r}})^\mathsf{T}\hat{\boldsymbol{v}} - \frac{1}{\eta_i A}\boldsymbol{M}_S\hat{\boldsymbol{S}}_i, \tag{31d}$$

$$\boldsymbol{M}_S\hat{\boldsymbol{S}} = \nabla\hat{W}_i(\hat{\boldsymbol{C}}), \tag{31e}$$

$$\boldsymbol{M}_S\hat{\boldsymbol{S}}_i = \nabla\hat{\tilde{W}}_i(\hat{\boldsymbol{C}}_i^{\mathrm{el}}), \tag{31f}$$

for $i = 1, \ldots, m$, as semi-discrete equations of motion where $\hat{\square}$ indicates nodal values. [7] The discrete version of the Hamiltonian

$$\hat{H}(\hat{\boldsymbol{x}}) = \frac{1}{2}\hat{\boldsymbol{v}}^\mathsf{T}\boldsymbol{M}_\rho\hat{\boldsymbol{v}} - \hat{\boldsymbol{r}}^\mathsf{T}\boldsymbol{M}\hat{\boldsymbol{b}} + \hat{W}(\hat{\boldsymbol{C}}) + \sum_{i=1}^m \hat{\tilde{W}}_i(\hat{\boldsymbol{C}}_i^{\mathrm{el}}) \tag{32}$$

with the states of the finite-dimensional model

$$\hat{\boldsymbol{x}} = (\hat{\boldsymbol{r}}, \hat{\boldsymbol{v}}, \hat{\boldsymbol{C}}, \hat{\boldsymbol{C}}_1^{\mathrm{el}}, \ldots, \hat{\boldsymbol{C}}_m^{\mathrm{el}}) \tag{33}$$

results from approximating (20) using the above ansatz functions. The discrete Hamiltonian $\hat{H}$ gives rise to the partial derivatives

$$\begin{aligned} \frac{\partial\hat{H}}{\partial\hat{\boldsymbol{r}}} &= -\boldsymbol{M}\hat{\boldsymbol{b}}, \quad \frac{\partial\hat{H}}{\partial\hat{\boldsymbol{C}}} = \nabla\hat{W}_i(\hat{\boldsymbol{C}}), \\ \frac{\partial\hat{H}}{\partial\hat{\boldsymbol{v}}} &= \boldsymbol{M}_\rho\hat{\boldsymbol{v}}, \quad \frac{\partial\hat{H}}{\partial\hat{\boldsymbol{C}}_i^{\mathrm{el}}} = \nabla\hat{\tilde{W}}_i(\hat{\boldsymbol{C}}_i^{\mathrm{el}}). \end{aligned} \tag{34}$$

We are now able to rewrite equations (31) as finite-dimensional PH system. Similar to (25), we obtain

$$\begin{aligned} \boldsymbol{E}\tfrac{\mathrm{d}}{\mathrm{d}t}\hat{\boldsymbol{x}} &= (\boldsymbol{J}(\hat{\boldsymbol{x}}) - \boldsymbol{R})\,\hat{\boldsymbol{z}} + \boldsymbol{B}\hat{\boldsymbol{u}}, \\ \hat{\boldsymbol{y}} &= \boldsymbol{B}^\mathsf{T}\hat{\boldsymbol{z}}, \end{aligned} \quad \text{and} \quad \boldsymbol{E}^\mathsf{T}\hat{\boldsymbol{z}} = \nabla\hat{H}(\hat{\boldsymbol{x}}), \tag{35}$$

in which $\boldsymbol{J}^\mathsf{T} = -\boldsymbol{J}$ and $\boldsymbol{R} = \boldsymbol{R}^\mathsf{T} \geq 0$. In detail, for the present problem we have

$$\boldsymbol{J}(\hat{\boldsymbol{x}}) = \begin{bmatrix} \boldsymbol{0} & \boldsymbol{I} & \boldsymbol{0} & \boldsymbol{0} \\ -\boldsymbol{I} & \boldsymbol{0} & -2\boldsymbol{K}(\hat{\boldsymbol{x}}) \cdots & -2\boldsymbol{K}(\hat{\boldsymbol{x}}) \\ \boldsymbol{0} & 2\boldsymbol{K}(\hat{\boldsymbol{x}})^\mathsf{T} & \boldsymbol{0} & \boldsymbol{0} \\ & \vdots & & \\ \boldsymbol{0} & 2\boldsymbol{K}(\hat{\boldsymbol{x}})^\mathsf{T} & \boldsymbol{0} & \boldsymbol{0} \end{bmatrix} \tag{36}$$

$$\hat{\boldsymbol{z}} = (-\boldsymbol{M}\hat{\boldsymbol{b}}, \hat{\boldsymbol{v}}, \frac{1}{2}\hat{\boldsymbol{S}}, \frac{1}{2}\hat{\boldsymbol{S}}_1, \ldots, \frac{1}{2}\hat{\boldsymbol{S}}_m), \tag{37}$$

$$\boldsymbol{R} = \mathrm{diag}\{\boldsymbol{0}, \boldsymbol{0}, \boldsymbol{0}, \frac{2}{\eta_1 A}\boldsymbol{M}_S, \ldots, \frac{2}{\eta_m A}\boldsymbol{M}_S\}, \tag{38}$$

$$\boldsymbol{E} = \mathrm{diag}\{\boldsymbol{I}, \boldsymbol{M}_\rho, \boldsymbol{M}_S, \boldsymbol{M}_S, \ldots, \boldsymbol{M}_S\}, \tag{39}$$

$$\boldsymbol{B}\hat{\boldsymbol{u}} = \boldsymbol{B}_\partial\hat{\boldsymbol{u}}_\partial. \tag{40}$$

Note that $\boldsymbol{E}^\mathsf{T} = \boldsymbol{E}$. In analogy to (19) and (29), the non-negative dissipated power is

$$\hat{D}(\hat{\boldsymbol{z}}) = \hat{\boldsymbol{z}} \cdot \boldsymbol{R}\hat{\boldsymbol{z}} = \sum_{i=1}^m \frac{1}{2\eta_i A}\hat{\boldsymbol{S}}_i^\mathsf{T}\boldsymbol{M}_S\hat{\boldsymbol{S}}_i \geq 0. \tag{41}$$

Correspondingly, the discrete power balance

$$\begin{aligned} \frac{\mathrm{d}}{\mathrm{d}t}\hat{H}(\hat{\boldsymbol{x}}) &= \nabla\hat{H}(\hat{\boldsymbol{x}}) \cdot \frac{\mathrm{d}}{\mathrm{d}t}\hat{\boldsymbol{x}} = \hat{\boldsymbol{z}} \cdot \boldsymbol{E}\frac{\mathrm{d}}{\mathrm{d}t}\hat{\boldsymbol{x}} \\ &= -\hat{\boldsymbol{z}} \cdot \boldsymbol{R}\hat{\boldsymbol{z}} + \hat{\boldsymbol{u}} \cdot \hat{\boldsymbol{y}} \leq \hat{\boldsymbol{u}} \cdot \hat{\boldsymbol{y}} \end{aligned} \tag{42}$$

expresses the passivity and dissipativity of the finite-dimensional model, which includes energy conservation for vanishing inputs and $\boldsymbol{R} = \boldsymbol{0}$.

3.2 Temporal discretization

Now, a suitable time discretization is applied to obtain a structure-preserving scheme, which extends the one in Kinon et al. (2023b). Consider a PH system of the general form (35) and let $\hat{\boldsymbol{x}}^n \approx \hat{\boldsymbol{x}}(t^n)$ at time $t^n = nh$ with constant time step sizes $h = t^{n+1} - t^n$. We propose an implicit one-step scheme given by

$$\begin{aligned} \boldsymbol{E}\left(\hat{\boldsymbol{x}}^{n+1} - \hat{\boldsymbol{x}}^n\right) &= h(\bar{\boldsymbol{J}} - \boldsymbol{R})\bar{\boldsymbol{z}} + h\,\boldsymbol{B}\bar{\boldsymbol{u}}, \\ \bar{\boldsymbol{y}} &= \boldsymbol{B}^\mathsf{T}\bar{\boldsymbol{z}}, \end{aligned} \tag{43}$$

and

$$\boldsymbol{E}^\mathsf{T}\bar{\boldsymbol{z}} = \overline{\nabla}\hat{H}(\hat{\boldsymbol{x}}^n, \hat{\boldsymbol{x}}^{n+1}), \tag{44}$$

where the solution via Newton's method is required in each time step. $\overline{\nabla}\hat{H}(\hat{\boldsymbol{x}}^n, \hat{\boldsymbol{x}}^{n+1})$ is a midpoint discrete derivative in the sense of Gonzalez (1996). It is a second order

[6] We use the notation $(a, b)_\Omega$ for a generalized inner product.

[7] See Kinon et al. (2023a) for formal expressions of the corresponding matrices and vectors.

perturbation to the midpoint evaluation of the analytical gradient and satisfies directionality and consistency, i.e.,

$$\overline{\nabla}\hat{H}(\hat{\boldsymbol{x}}^n,\hat{\boldsymbol{x}}^{n+1})^{\mathsf{T}}\left(\hat{\boldsymbol{x}}^{n+1}-\hat{\boldsymbol{x}}^n\right)=\hat{H}(\hat{\boldsymbol{x}}^{n+1})-\hat{H}(\hat{\boldsymbol{x}}^n), \quad (45)$$

$$\overline{\nabla}\hat{H}(\hat{\boldsymbol{x}}^n,\hat{\boldsymbol{x}}^n)=\nabla\hat{H}(\hat{\boldsymbol{x}}^n), \quad (46)$$

for arbitrary $\hat{\boldsymbol{x}}^n,\hat{\boldsymbol{x}}^{n+1}$. For the system at hand, the discrete gradient can be designed analogously to Kinon et al. (2023a). Using (45) and performing similar manipulations as in (42) we obtain the discrete-time power balance

$$\hat{H}^{n+1}-\hat{H}^n=h\,\bar{\boldsymbol{u}}\cdot\bar{\boldsymbol{y}}-h\bar{D}\le h\,\bar{\boldsymbol{u}}\cdot\bar{\boldsymbol{y}}, \quad (47)$$

with the non-negative discrete-time dissipation function

$$\bar{D}=\bar{\boldsymbol{z}}^{\mathsf{T}}\boldsymbol{R}\bar{\boldsymbol{z}}\ge 0, \quad (48)$$

showing that the proposed integrator exhibits discrete-time passivity and dissipativity (including energy-conservation for $\bar{\boldsymbol{u}}=\boldsymbol{0}$, $\boldsymbol{R}=\boldsymbol{0}$). Discrete gradient methods are known for desirable robustness and stability properties.

Remark 2. These properties hold regardless of the specific choices for the matrix- and vector-evaluations. As in Kinon et al. (2023b), we choose $\bar{\boldsymbol{J}}=\boldsymbol{J}(\hat{\boldsymbol{x}}^{n+1/2})$ based on $\hat{\boldsymbol{x}}^{n+1/2}=\frac{1}{2}(\hat{\boldsymbol{x}}^{n+1}+\hat{\boldsymbol{x}}^n)$, as well as $\bar{\boldsymbol{u}}=\hat{\boldsymbol{u}}(t^{n+1/2})$ such that $\bar{\boldsymbol{y}}\approx\hat{\boldsymbol{y}}(t^{n+1/2})$, to obtain a symmetric method.

Remark 3. Our method falls into the definition of a *discrete-gradient pair* (Schulze, 2023, Sec. 4) with

$$\bar{\boldsymbol{E}}=\boldsymbol{E},\qquad \bar{\boldsymbol{z}}(\hat{\boldsymbol{x}}^n,\hat{\boldsymbol{x}}^{n+1})=\boldsymbol{E}^{-\mathsf{T}}\overline{\nabla}\hat{H}(\hat{\boldsymbol{x}}^n,\hat{\boldsymbol{x}}^{n+1}), \quad (49)$$

satisfying the three conditions in Schulze (2023). This follows directly from the definition as well as (45) and (46). Despite using the midpoint discrete gradient, the proposed method differs from the *midpoint discrete-gradient pair* in Schulze (2023).

4. NUMERICAL EXAMPLE

We investigate the planar motion of a string made of rubber-like material ($E=18400\,\mathrm{N/m^2}$, $\rho=920\,\mathrm{kg/m^3}$) with circular cross section (radius $r=0.0186\,\mathrm{m}$). Without loss of generality, we consider the common *Zener model* (the one-dimensional *standard solid*, see Simo and Hughes (2006)), which is the generalized Maxwell model with $m=1$. For further parameters see Table 1.

It is discretized in space with $n_{\mathrm{el}}=10$ finite elements and numerical quadrature of the integrals considered two Gauss points per element. Further parameters are shown in Table 1. Specifying the reference configuration Ω by

$$\boldsymbol{r}_0(s)=s\begin{bmatrix}0\\-1\end{bmatrix},\quad \boldsymbol{v}_0(s)=\boldsymbol{0},\quad C_0(s)=1, \quad (50)$$

we compute the static equilibrium in this vertical position determined by gravity $\boldsymbol{b}=-9.81\rho A\boldsymbol{e}_2$. To this end, the creeping process is simulated for a period of 10 s, where inertial forces are neglected. From this approximate steady state (marked as black in Fig. 3), we perform the dynamics simulation, where Newton's method was used with a residual tolerance of $\varepsilon=10^{-10}$. The finite element code `moofeKIT` has been used, see Franke et al. (2023). Considering mixed BCs [8]

$$\begin{aligned} &r_2(s=0,t)=0,\quad v_2(s=0,t)=0,\quad \forall t\\ &\boldsymbol{F}_{\mathrm{N}}=\rho A\begin{bmatrix}1\\0\end{bmatrix}\sin\left(\pi\frac{t}{2}\right),\qquad t\in[0,4]\,, \end{aligned} \quad (51)$$

[8] Here, homogeneous Dirichlet BCs are enforced directly into the ansatz functions. In general, enforcing non-homogeneous mixed BCs for PHS requires further approaches, see Brugnoli et al. (2022).

Table 1. Simulation parameters

L [m]	EA, E_1A [N]	ρA [kg/m]	$\eta_1 A$ [Ns]	h [s]	$\mathbb{T}$ [s]
1	10	1	0.4	$5\cdot10^{-2}$	$[0,6]$

the homogeneous Dirichlet BCs are given by fixing the vertical component of the upper end of the string, and the non-homogeneous Neumann BC acts at the upper end ($s=0$) of the string during a loading phase in horizontal direction. Due to a free lower end, we consider homogeneous Neumann conditions at $s=L$. After $t=4$, the system is closed. Snapshots of the motion are displayed in Fig. 3 for $t\in\{0,0.4,\dots 3.6,4\}$ s.

The dissipated work in each time step can be seen in Fig. 4 and verifies (48). During the loading phase, the power-transmission through the boundaries can be observed in Fig. 5. After the loading phase, our discrete gradient method (labeled "DG") captures the dissipativity down to a level of machine precision. Using the well-known implicit midpoint rule (labeled "MP") is not as accurate due to the nonlinear material (5). The difference between MP and DG is even more distinct for examples, which induce more elongation, see Kinon et al. (2023a).

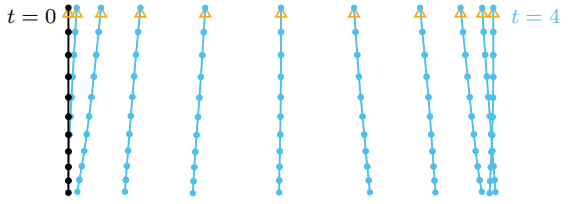

Fig. 3. Initial configuration and snapshots

5. CONCLUSION & OUTLOOK

In this work, we have proposed a new approach for the simulation of hyperelastic and viscously damped strings, which additionally enjoys a port-Hamiltonian structure.

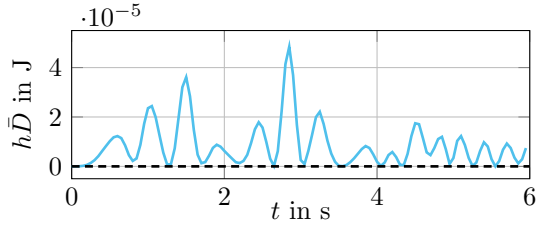

Fig. 4. Discrete dissipated work $h\bar{D}$

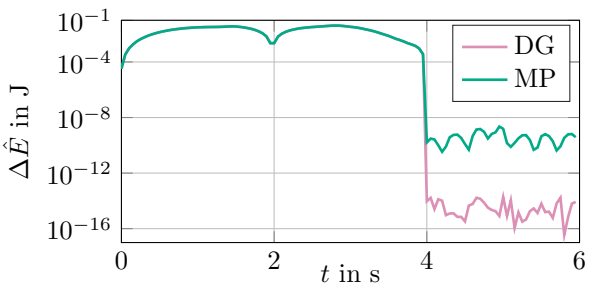

Fig. 5. Discrete increments $\Delta\hat{E}:=|\hat{H}^{n+1}-\hat{H}^n+h\bar{D}|$

The infinite-dimensional model is nonlinear and dissipative and features boundary input/output ports. It could be shown that dissipation in the sense of a generalized Maxwell model can be provided via power-preserving PH connection of two subsystems. Subsequently, we have demonstrated advantageous properties of both spatial and temporal discretization techniques, which are structure-preserving: a mixed finite element approach in space, yielding a finite-dimensional PH state space model, and a discrete-gradient based integrator in time, inheriting the passivity of the original system. Eventually, the behavior of the model could be showcased in an example simulation, demonstrating also the advantages with respect to a standard time discretization. Future research directions may investigate the usage of this model for control design as well as model order reduction.

ACKNOWLEDGEMENTS

PLK acknowledges interesting discussions with P. Schulze (TU Berlin) and M. Hille (KIT). We thank F. Zähringer and M. Franke (both KIT) for the support using `moofeKIT`.

REFERENCES

Bauchau, O.A. and Nemani, N. (2021). Modeling viscoelastic behavior in flexible multibody systems. *Multibody Syst. Dyn.*, 51, 159–194.

Brugnoli, A., Haine, G., and Matignon, D. (2022). Explicit structure-preserving discretization of port-Hamiltonian systems with mixed boundary control. *IFAC-PapersOnLine*, 55, 418–423.

Brugnoli, A., Rashad, R., Califano, F., Stramigioli, S., and Matignon, D. (2021). Mixed finite elements for port-Hamiltonian models of von Kármán beams. *IFAC-PapersOnLine*, 54(19), 186–191.

Cardoso-Ribeiro, F.L., Matignon, D., and Lefèvre, L. (2021). A partitioned finite element method for power-preserving discretization of open systems of conservation laws. *IMA J. Math. Control. Inf.*, 38(2), 493–533.

Duindam, V., Macchelli, A., Stramigioli, S., and Bruyninckx, H. (2009). *Modeling and control of complex physical systems: The port-Hamiltonian approach*. Springer, Berlin, Heidelberg.

Franke, M., Zähringer, F., Hille, M., Kinon, P.L., and Reiff, P. (2023). MoofeKIT: MATLAB object-oriented finite element KIT. doi:10.5281/zenodo.10416814.

Gonzalez, O. (1996). Time integration and discrete Hamiltonian systems. *J. Nonlinear Sci.*, 6, 449–467.

Kinon, P.L., Thoma, T., Betsch, P., and Kotyczka, P. (2023a). Port-Hamiltonian formulation and structure-preserving discretization of hyperelastic strings. In *Proceedings of the 11th ECCOMAS Thematic Conference on Multibody Dynamics*, 1–10. Lisbon, Portugal.

Kinon, P.L., Thoma, T., Betsch, P., and Kotyczka, P. (2023b). Discrete nonlinear elastodynamics in a port-Hamiltonian framework. *PAMM*, 23(3), e202300144.

Linn, J., Lang, H., and Tuganov, A. (2013). Geometrically exact Cosserat rods with Kelvin–Voigt type viscous damping. *Mech. Sci.*, 4(1), 79–96.

Mehrmann, V. and Morandin, R. (2019). Structure-preserving discretization for port-Hamiltonian descriptor systems. In *Proceedings of the 58th IEEE Conference on Decision and Control*, 6863–6868. Nice, France.

Mehrmann, V. and Zwart, H. (2024). Abstract dissipative Hamiltonian differential-algebraic equations are everywhere. *arXiv:2311.03091 [math.FA]*. doi: 10.48550/arXiv.2311.03091.

Ponce, C., Wu, Y., Gorrec, Y.L., and Ramirez, H. (2023). Port-Hamiltonian modeling of multidimensional flexible mechanical structures defined by linear elastic relations. *arXiv:2311.03796 [math.DS]*. doi: 10.48550/arXiv.2311.03796.

Rashad, R., Califano, F., van der Schaft, A., and Stramigioli, S. (2020). Twenty years of distributed port-Hamiltonian systems: A literature review. *IMA J. Math. Control. Inf.*, 37(4), 1400–1422.

Schulze, P. (2023). Structure-preserving time discretization of port-Hamiltonian systems via discrete gradient pairs. *arXiv:2311.00403 [math.NA]*. doi: 10.48550/arXiv.2311.00403.

Simo, J.C. and Hughes, T.J. (2006). *Computational inelasticity*, volume 7. Springer, New York.

Ströhle, T. and Betsch, P. (2022). A simultaneous space-time discretization approach to the inverse dynamics of geometrically exact strings. *Int. J. Numer. Methods Eng.*, 123(11), 2573–2609.

Thoma, T. and Kotyczka, P. (2022). Port-Hamiltonian FE models for filaments. *IFAC-PapersOnLine*, 55(30), 353–358.

Appendix A. PH-PDAE CASE

By demanding the inextensibility constraint $C = 1$ for rigid strings or by time-differentiation $\partial_s \boldsymbol{r} \cdot \partial_s \boldsymbol{v} = 0$, one obtains similarly the PH differential-algebraic equations (25) with Lagrange multipliers $\xi \in \mathbb{R}$. They represent the reaction stress enforcing inextensibility and take part in $\boldsymbol{z} = (-\boldsymbol{b}, \boldsymbol{v}, 1/2\xi)$. Moreover, $\mathcal{E} = \operatorname{diag}\{\boldsymbol{I}, \rho A \boldsymbol{I}, 0\}$ is singular, $\mathcal{R} = 0$ and $\delta_C H = 0$. This model is equivalent to the one presented in Thoma and Kotyczka (2022).

Appendix B. CANONICAL CASE

An alternative PH representation for hyperelastic, geometrically exact strings can be obtained by choosing the states $\boldsymbol{x} = (\boldsymbol{p}, \boldsymbol{q}, \boldsymbol{r}) := (\rho A \dot{\boldsymbol{r}}, \partial_s \boldsymbol{r}, \boldsymbol{r})$ defining the Hamiltonian

$$H[\boldsymbol{x}] = \int_\Omega \left(U(\boldsymbol{q}) - \boldsymbol{r} \cdot \boldsymbol{b} + \frac{1}{2\rho A} \boldsymbol{p} \cdot \boldsymbol{p} \right) \mathrm{d}s \tag{B.1}$$

with the stored energy density $U(\boldsymbol{q}) = W(C)$. The efforts are obtained as

$$\delta_{\boldsymbol{p}} H = (\rho A)^{-1} \boldsymbol{p}, \ \delta_{\boldsymbol{q}} H = \nabla U(\boldsymbol{q}) =: \boldsymbol{n}_{\mathrm{el}}(\boldsymbol{q}), \ \delta_{\boldsymbol{r}} H = -\boldsymbol{b}. \tag{B.2}$$

The second relation can be verified by chain rule

$$\nabla U(\boldsymbol{q}) = \partial_{\boldsymbol{q}} W(C) = W'(C) \nabla C(\boldsymbol{q}) = S \partial_s \boldsymbol{r}. \tag{B.3}$$

Eventually, the state differential equations [9] are given by $\dot{\boldsymbol{x}} = \mathcal{J} \delta_{\boldsymbol{x}} H$ with the formally skew-adjoint operator

$$\mathcal{J} = \begin{bmatrix} 0 & \partial_s \square & -\boldsymbol{I} \\ \partial_s \square & 0 & 0 \\ \boldsymbol{I} & 0 & 0 \end{bmatrix}. \tag{B.4}$$

[9] This model should also be deducible using an approach extending the work by Ponce et al. (2023) to nonquadratic Hamiltonians.